

Strain localization due to structural in-homogeneities in the Central European Basin System

Mauro Cacace · Ulf Bayer · Anna Maria Marotta

Received: 18 October 2006 / Accepted: 16 April 2007 / Published online: 22 May 2007
© Springer-Verlag 2007

Abstract The large-scale crustal deformations observed in the Central European Basin System (CEBS) are the result of the interplay between several controlling factors, among which lateral rheological heterogeneities play a key role. We present a finite-element integral thin sheet model of stress and strain distribution within the CEBS. Unlike many previous models, this study is based on thermo-mechanical data to quantify the impact of lateral contrasts on the tectonic deformation. Elasto-plastic material behaviour is used for both the mantle and the crust, and the effects of the sedimentary fill are also investigated. The consistency of model results is ensured through comparisons with observed data. The results resemble the present-day dynamics and kinematics when: (1) a weak granite-like lower crust below the Elbe Fault System is modelled in contrast to a stronger lower crust in the area extending north of the Elbe Line throughout the Baltic region; and (2) a transition domain in the upper mantle is considered between the shallow mantle of the Variscan domain and the deep mantle beneath the East European Craton (EEC), extending from the Elbe Line in the south till the Tornquist Zone. The strain localizations observed along these structural contrasts strongly enhance the dominant role played by large structural domains in stiffening the propagation of tectonic deformation and in controlling the basin formation and the evolution in the CEBS.

Keywords Central European Basin System · Rheological heterogeneities · Thin sheet approach · Stress and strain localization

Abbreviations

CEBS	Central European Basin System
NDB	Norwegian-Danish Basin
NGB	North German Basin
PT	Polish Trough
TZ	Tornquist Zone
STZ	Sorgenfrey-Tornquist-Zone
TTZ	Teysserie-Tornquist-Zone
RFH	Ringkøbing-Fyn-High
EL	Elbe Line
EFS	Elbe Fault System
CG	Central Graben
GG	Glückstadt Graben
HG	Horn Graben

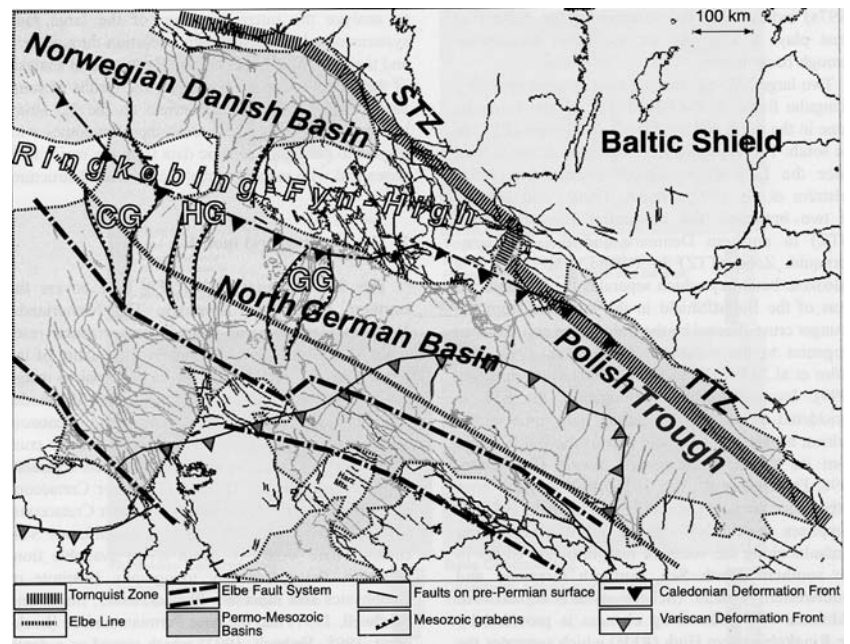
Introduction

The Central European Basin System (CEBS) covers a large area from the North Sea to Poland and from Denmark to North Germany. It is composed of two main basins, the Southern Permian Basin and the Northern Permian Basin. These two basins are superimposed on different continental crustal domains with Precambrian to Variscan consolidation ages. The CEBS includes a number of sedimentary sub-basins, among which the major ones are: the Norwegian-Danish Basin (NDB), the North German Basin (NGB), and the Polish Trough (PT) (Fig. 1). The formation and further development of these

M. Cacace (✉) · U. Bayer
GeoForschungZentrum (GFZ) Potsdam, Sec. 4.3,
Telegrafenberg, 14473 Potsdam, Germany
e-mail: cacace@gfz-potsdam.de

A. M. Marotta
Department of Earth Sciences, Sec. Geophysics,
University of Milan, Milan, Italy

Fig. 1 Structural map of the Central European Basin System (Vejbaek 1997; Lockhorst 1998; NW European Gas Atlas; Scheck-Wenderoth et al. 2002). The major elements shown are: (1) the Tornquist Zone (TZ) consisting of the Sorgenfrey-Tornquist-Zone (STZ) and the Teysserie-Tornquist-Zone (TTZ). (2) The Ringkøbing-Fyn-High (RFH). (3) The Elbe Fault System (EFS). (4) The N-S-striking Mesozoic Grabens: the Central Graben (CG), the Horn Graben (HG) and the Glückstadt Graben (GG)



sub-basins are similar and can be summarized in a three step process (Ziegler 1990; Scheck-Wenderoth and Lamarche 2005): after basins formation in the Late Carboniferous–Early Permian time, accompanied by intense magmatism, a period of thermal subsidence, as predominantly assumed, dominated during latest Late Paleozoic and earliest Triassic. The Late Triassic to Late Jurassic evolution was characterized by a rifting phase followed by Cretaceous–Early Cenozoic inversion and a final subsidence stage in the Cenozoic. Studies from different parts of the CEBS (Vejbaek 1997; Berthelsen 1998; Scheck-Wenderoth et al. 2002) have suggested that basin formation and evolution was mainly controlled by the presence of deep reaching zones of lithospheric weakness. Bayer et al. (1997) have related these zones of observed stress and strain localization with the underlying structure of the lower crust or the lithospheric mantle, where areas of reduced viscosity or elevated temperature can play a key role in focusing deformation. In addition, basins evolution was also strongly influenced by the growth of salt structures (Maystrenko et al. 2005). For example, local salt movements strongly affect and even determine the stress pattern in the overburden (Bayer et al. 1999; Marotta et al. 2000). Moreover, the CEBS is located over a variety of crustal structures which have been tectonically reactivated through time. Dominant are NW-SE striking elements (Fig. 1): (1) the Tornquist Zone (STZ and TTZ) in the north-eastern part of the study area, (2) the Ringkøbing-Fyn-High (RFH), a structural high consisting of faulted blocks separating the Norwegian-Danish Basin from the North German Basin; (3) the Elbe Line (EL) which most probably acts as the southernmost border of the Baltic

domain; and (4) the Elbe Fault System (EFS), a weak upper crustal domain active since Late Carboniferous times where strain localization was repeatedly observed and may be ongoing (Mattern 1996; Scheck-Wenderoth et al. 2002). Other important structures are N-S striking grabens which formed during the Mesozoic differentiation phase of the CEBS. The largest of these are the Central Graben (CG), the Glückstadt Graben (GG) and the Horn Graben (HG). Due to the superposition of all these distinctive elements, the CEBS shows a very complex structural setting. Regarding basin evolution, new information is now available concerning crustal and shallow mantle structures as derived from gravity modelling (Yegorova et al. 2007), deep seismic experiments (MONA-LISA Group 1997; DEKORP-BASIN Group 1999; Guterch et al. 1999), seismic tomography (Gregeresen et al. 2002), structural crustal modelling (Gemmer and Nielsen 2001; Scheck-Wenderoth and Lamarche 2005), and stress field modelling (Kaiser et al. 2005). Based on all these results, we used a thin sheet integral modelling approach to investigate the influence of the deep crustal structures and their related rheologies. We tested our results on two different independent observable parameters, the deformation pattern and stress field variations. In order to understand the interconnections between these elements we did not introduce any pre-defined faults in the models as in other studies (Kaiser et al. 2005). However, we relied on previous numerical results for choosing the material parameters and the boundary conditions (Marotta and Sabadini 2003; Marotta et al. 2004; Marotta 2005; Yegorova et al. submitted; Scheck-Wenderoth et al. 2002; Scheck-Wenderoth and Lamarche 2005).

Horizontal deformation velocity field and strain rates

In order to test and quantify the consistency of the numerical model, the obtained results were compared with different types of observable data sets. The first one is the horizontal deformation velocity field. This data set is based on the last ten years of GPS observations which were used to define the ITRF2000 velocity solution database (Altamini et al. 2002). In order to compare the results of our model with geodetic data, the deformation is represented by the horizontal eigenvectors of the strain rate tensor. As already observed in previous work by Marotta (2005), the comparison between the geodetic and the model eigenvalues allows to quantify the quality of the model. Figure 2 shows the horizontal strain-rate eigenvectors derived from ITRF2000 solutions in Central Europe (black indicating extension, grey compression) computed for triangular domains following the approach of Devoti et al. (2002).

Fig. 2 Triangular horizontal strain-rate eigenvectors derived from the ITRF2000 solutions in Central Europe (Black indicates extension, and grey compression). The thinner black and grey coloured lines in the left angle indicate non-significant strain rates (modified from Marotta 2005)

The main features are (1) a general SW-NE-directed compression in opposition to a SE-NW-directed extension, and (2) while at high latitudes extension dominates over compression, at middle latitudes the two types of deformation styles are comparable.

Stress field pattern

The second data set used to test the quality of the results is represented by the stress field as obtained from the ‘‘World Stress Map Project’’ (Reinecker et al. 2005). This database provides the direction of the maximum horizontal stress and the related regime as derived from several sources, such as earthquake focal mechanisms, young geological indicators and borehole breakouts (Fig. 3). These data can be compared to the maximum horizontal component of the stress tensor derived from the model. As usually assumed in any continuum approach to model continental deformation, the

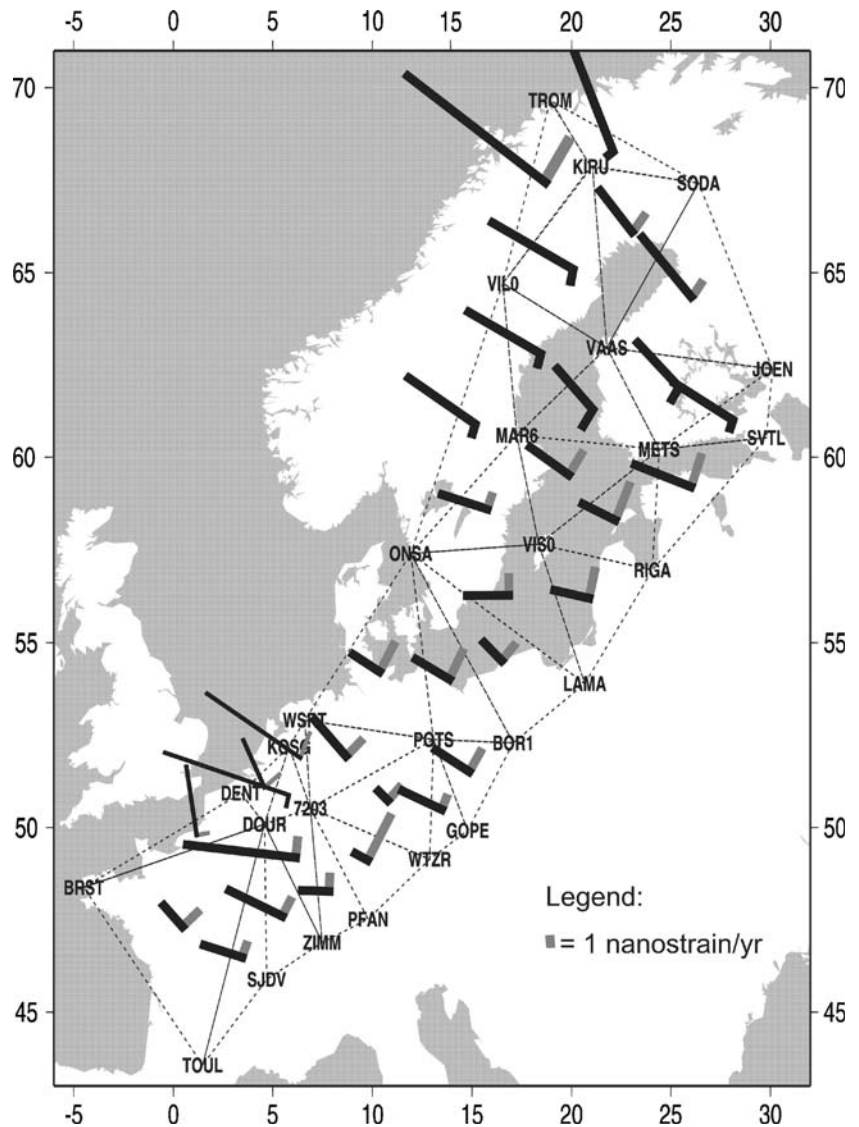
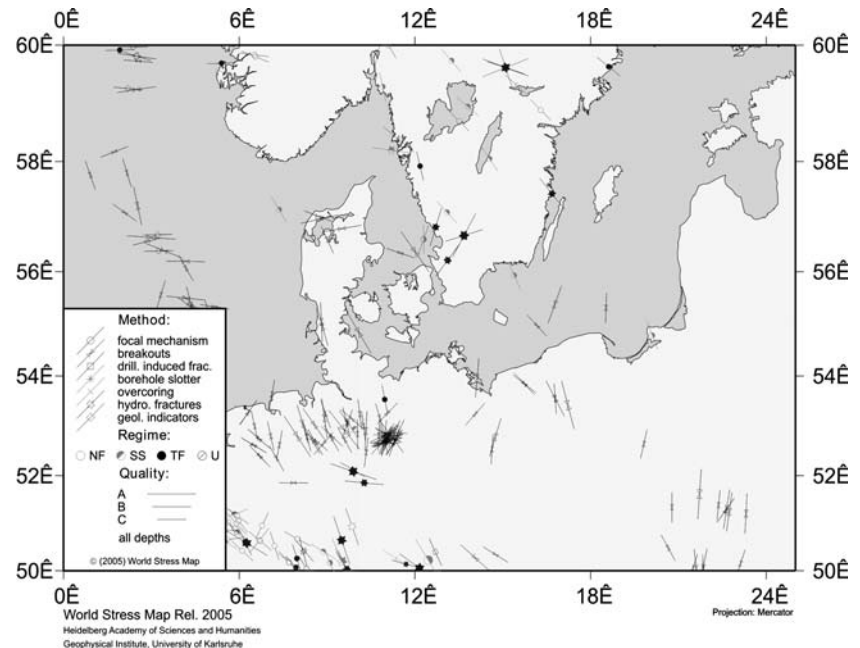


Fig. 3 Map showing the direction of the largest horizontal stress for the area under investigation (Reinecker et al. 2005, ‘‘The release 2005 of the World Stress Map’’)



lithosphere is regarded as an isotropic medium. This reasonable assumption is reflected by a rheological law which explicitly links strain rates with stress components. Consequently, directions of stresses and strain rate eigenvectors coincide. Thus, after having obtained the horizontal velocity deformation field, the largest horizontal component of the stress tensor is easily estimated from the horizontal gradients of the velocity field and from the nodal values of the viscosity implemented in the thin sheet calculations (Ranalli 1995; Turcotte and Schubert 2002).

Model set up

A spherical thin sheet approach was adopted to calculate the deformation and the stresses inside the Central European Basin System, based on Marotta et al. (2004) where a detailed description of the mathematical formulation of the method is given. The domain of the CEBS was discretized by 2,000 spherical finite triangular elements, Fig. 4a. Our mesh was obtained by refining of the original grid of Marotta et al. (2004), and then it was adapted to the local frame. The model area covers a region extending from the 50°N to the 60°N parallel and from the 0°E to the 25.5°E meridian. We considered the asthenosphere as an inviscid element thus assuring a stress-free condition at the base of the plate. The lithosphere consists of three main vertical structural layers, the sediments which cover the basin area, the crust (further divided in two layers) and the mantle. Each domain may behave in a brittle, ductile or elastic manner in relation to the thermal state and the local strain rate. For brittle failure plastic deformation is used, therefore all properties depend on pressure but not on temperature or rock type (Byerlee

1978; Cloetingh and Burov 1996). Due to the thin sheet assumption of plain stress, it follows that one of the principal stresses coincides with the vertical stress. Under this condition, known as ‘‘Andersonian stress regime’’, the brittle yield strength, σ_B , follows Byerlee’s law (Ranalli 1995; Turcotte and Schubert 2002):

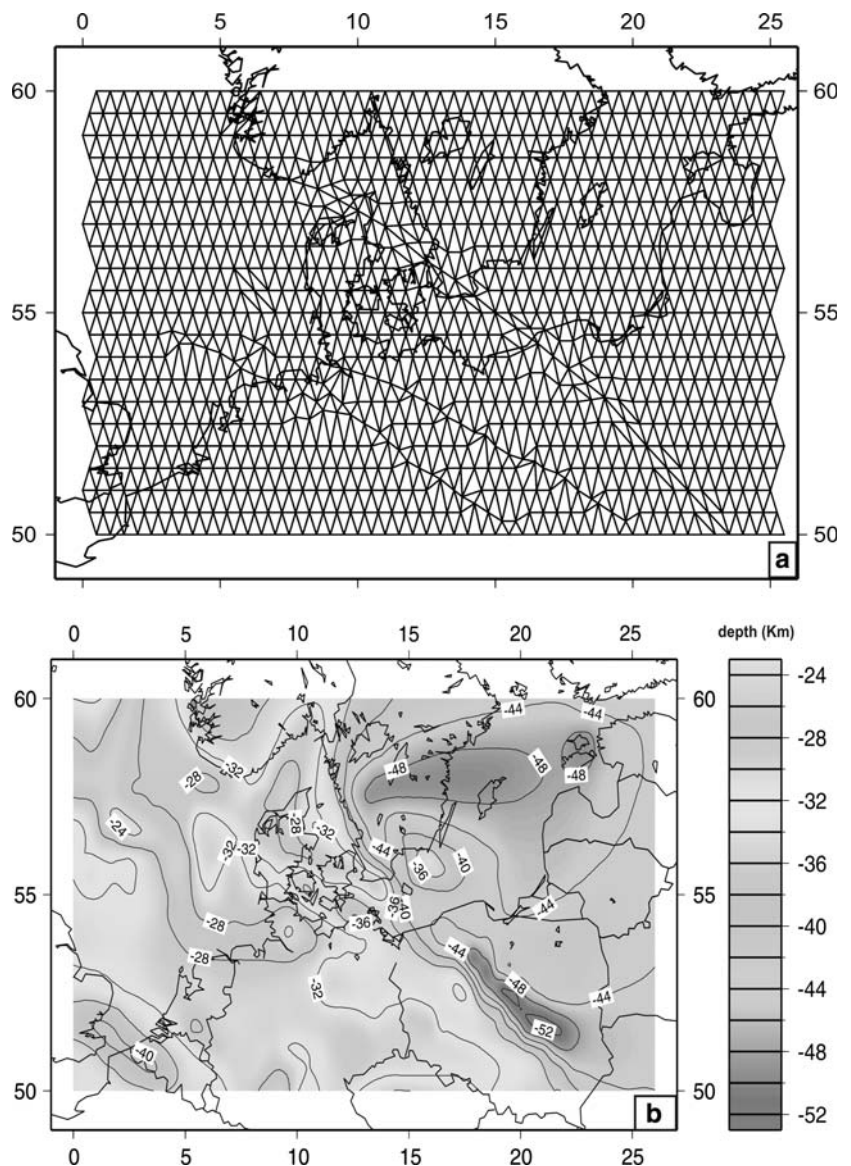
$$\sigma_B = (\sigma_H - \sigma_V)_B = \beta \cdot z;$$

where σ_H and σ_V represent the maximum and the minimum principal stress respectively, z is the depth while β is the brittle failure coefficient depending on the type of fault, the angle of fracture and the pore pressure. Its value amounts 16 Mpa km^{-1} for extensional setting and 40 Mpa km^{-1} for compression (Lynch and Morgan 1987; Jiménez-Munt et al. 2005). At high temperatures deformation within the lithosphere is dominated by creep mechanisms. Laboratory studies have demonstrated that the ductile yield strength is a function of a power of the strain rate and depends strongly on temperature and rock type (e.g. Goetze and Evans 1979; Ranalli 1995). Following these suggestions, to model ductile behaviour a power law steady-state flow creep relation is assumed (e.g. Ranalli 1995; Turcotte and Schubert 2002):

$$\sigma_D = (\sigma_H - \sigma_V)_D = \left(\frac{\dot{\epsilon}}{\dot{\epsilon}_0}\right)^{\frac{1}{n}} \cdot \exp\left(\frac{E}{nRT}\right)$$

where $\dot{\epsilon}$ is the effective strain rate given by the second invariant of the strain tensor, R is the gas constant, T is the absolute temperature and $\dot{\epsilon}_0$, n , E are material constants depending on the rock type. The steady-state power law flow creep equation indicates that the critical

Fig. 4 a Finite element grid adopted for the tectonic predictions in the study. **b** Crustal thickness variation used in the analysis. Adapted to the domain from the European Moho base-map, Ziegler and Dèzes (2005)



differential stresses decrease exponentially with increasing temperature. However, above a critical stress ductile deformation becomes to be governed by dislocation processes. Following previous works (e.g. Weertman and Weertman 1975; Goetze and Evans 1979), it is commonly assumed for olivine that for applied stresses higher than 200 MPa in magnitude, the governing equation takes the form of the so-called Dorn law (Weertman and Weertman 1975; Ranalli 1995; Turcotte and Schubert 2002):

$$\sigma_D = \sigma_0 \left\{ 1 - \sqrt{\left[\left(\frac{RT}{E_A} \right) \cdot \ln \left(\frac{\epsilon_D}{\dot{\epsilon}} \right) \right]} \right\}; \quad \sigma \geq 2000 \text{ MPa}$$

where σ_0 , E_A and ϵ_D are flow parameters. The yield strength envelope, σ_Y , is given by a contour function assuming the form:

$$\sigma_Y = \pm \min\{|\sigma_B|; |\sigma_D|\},$$

which is positive for extension and negative for compression. The regional strain rate ranges between 10^{-16} and 10^{-14} s^{-1} for both compressional and extensional settings (Molnar and Tapponier 1981; Cloetingh and Burov 1996). As demonstrated in previous studies (Lankreijer et al. 1997; Marotta et al. 2000), the results are not strongly affected by changes in strain rate values, because strain rates within one order of magnitude provide changes less than 10%. The effective viscosity (η) is calculated from the depth integral of the yield strength envelope and is a function of the temperature and local strain rate. The boundary conditions imposed on the model are given in terms of crustal thickness and horizontal velocity (Fig. 4a, b). For crustal thickness, the European Moho

contour map published by Ziegler and Dèzes (2005) was adapted to the size of the study area and to the nodes of our triangular mesh. Although different boundary velocity conditions play an important role in terms of stresses and strains, a detailed analysis of their influences is beyond the present purpose of the paper. Moreover, the results of Marotta et al. (2004) suggest that amplitudes and directions of predicted horizontal velocities at sites located well away from plate boundaries are more sensitive to the adopted modelling parameters than to slightly changeable boundary conditions. Consequently, in order to better constrain the role of lithospheric structures, all the calculations were performed imposing one set of fixed velocity boundary conditions to the integral grid. To determine the suitable boundary conditions, the nodal values of horizontal deformation velocity as obtained from the reference model of Marotta et al. (2004) were adjusted to our new grid. The applied velocity boundary conditions within the study performed by Marotta et al. (2004) were modelled relative to an assumed fixed Eurasian plate and comprised (Fig. 5):

1. Ridge push forces acting along the North Atlantic Ridge. These forces were parameterized in terms of velocity boundary conditions applied along the ridge. In this way, horizontal velocities simulate the line forces acting along the plate boundary, thick grey arrows of Fig. 5. The line force normal to the ridge was calculated from the eigenvalues of the stress tensor within the elements used to define the ridge (Richardson et al. 1979). Velocities at the boundaries range between a minimum of about 1 mm/year to a maximum value of 5 mm/year. Accordingly, the range of predicted push forces along the westernmost part of the Atlantic Ridge varies from about 10^{12} N/m for an imposed velocity boundary condition of about 1 mm/year up to a maximum of about 10^{13} N/m for an imposed velocity boundary condition of 5 mm/year.
2. Effects related with the continental convergence between the African plate and the Eurasian plate, thin black arrows of Fig. 5. The velocity of Africa relative to Eurasia was constrained from the data derived from NUVEL-1A whose patterns resemble a counter-clockwise rotation of Africa with respect to Europe superimposed on a continental convergence between the two plates of the order of 1 cm/year.
3. Effects related to subduction forces along the Aegean trench, thin white arrows of Fig. 5. Velocities values used were the same as geodetically determined by McClusky et al. (2000).

The eastern boundary of the model was kept fixed imposing a shear stress free condition, black circles of Fig. 5.

In choosing the set of velocity boundary conditions to impose on our study area, the effects related to the Middle

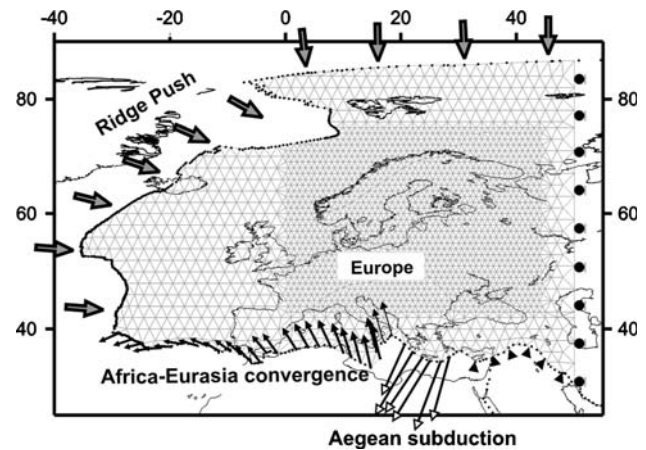


Fig. 5 Finite element grid adopted for the tectonic predictions as described in the modelling study of Marotta et al. (2004). The *thick grey arrows* along the western and northern boundaries represent ridge push forces from the North Atlantic. The counter-clockwise rotation of the African plate with respect the Eurasian plate is reflected by the *thin black arrows* along the south-western boundary. The velocities at the Aegean Trench, *thin white arrows*, were geodetically determined by McClusky et al. (2000) and reflect the horizontal component of the trench subduction forces. The southern border between the model domain and the Arabian region is held fixed (*black triangles*), while the eastern boundary is assumed to be shear stress free (*black dots*)

Atlantic spreading were not taken into account, whereas those related with Africa-Eurasia collision as well as with the trench Aegean subduction were inserted. Our choice is based on the fact that (1) this type of boundary setting revealed to give the best fit in the reference model of Marotta et al. (2004), and (2) the present-day deformation pattern of the CEBS was mainly caused by collision-induced compressive stresses.

The velocity field was then approximated by linear polynomial interpolating functions and numerical integration was performed by Gaussian quadrature with 7 integration points for each element. In relation to the reference model, the modifications can be summarized as follows: (1) we avoided any oversimplification which can limit the capability of reproducing the effects due to variation in crustal and mantle thickness; (2) lateral contrasts were inserted in the most realistic manner following the information derived from different previous studies; (3) a coupled set of thermo-mechanical equations were used as governing ones.

Crustal and lithospheric mantle thickness variations

In the thin sheet approach the lithosphere is generally treated as one viscous layer or as two layers, mantle and crust, with constant or slightly variable thickness and vertically-averaged rheological properties. Despite the

successes reached in reproducing the general stress trend in Europe (e.g. Marotta et al. 2004), the oversimplifications included in these models turned out to be a limit in modelling tectonic scenarios in which depth related processes play an important role. Considering the Moho map (Ziegler and Dèzes 2005), it is evident that the CEBS is characterized by variable crustal thickness ranging from currently believed 25 km in its central part down to 48–50 km in the Baltic and East European Craton (EEC). Furthermore, the internal crustal structure is complicated by a thick sequence of sedimentary layers of different age (Ziegler 1990; Bayer et al. 1999; Krawczyk et al. 2002; Scheck-Wenderoth and Lamarche 2005; Majdanski et al. 2006). Going deeper, the asthenosphere–lithosphere thermo-mechanical boundary seems to behave almost similar to the Moho discontinuity, deepening below the EEC domain (Gregersen et al. 2002). As well documented from large seismic experiments (MONA-LISA Group 1997; DEKORP-BASIN Group 1999) and gravity modelling (Yegorowa et al. 2007), all these features are related to both lateral and vertical changes in geophysical properties. We performed several models for reproducing all the elements described in a stepwise approach in order to quantify their role in deformation.

Lateral rheological contrasts and thermal effects

Lateral structural contrasts have been incorporated in some of the previous models in terms of lateral variations of the Argand number, A_r (England and Houseman 1985; Marotta et al. 2002; Jimènez-Munt et al. 2005). This number provides a measure of the relative importance of viscous and buoyancy forces, and includes the vertically averaged dependence of the viscosity on temperature and lithospheric composition. Its value varies between 0 (for a strong lithosphere) and 50 (for a very soft one), but the parameter is not always consistent with experimentally observed rock properties (England and Houseman 1989; Jimènez-Munt et al. 2005). Moreover, as widely debated by several authors in the past (England and Houseman 1985; Tomasi et al. 1995; Ranalli 1995) the viscosity has a strong dependence on the temperature profile, which controls the rheology of the Earth. Several studies (Bijwaard et al. 1998; Goes et al. 2000) have demonstrated the presence of 100–300°C fluctuation in the temperature under north-western Europe due to lithospheric mantle thickness variations. This inferred anomalous large scale mantle structure strongly influences the intraplate tectonic activity and may also cause variations in stress and tectonic style. Despite of this fact, most of the previous thin sheet models did not include any thermal calculations or tried to incorporate the temperature-related effects more or less arbitrarily. In order

to avoid all these limitations, we implemented a three dimensional thermal conductive model which allows to solve for the temperature field with depth. The most important rock properties, such as radiogenic heat production, thermal conductivity and volumetric expansion coefficient, as derived from several localized studies for the different sub-parts of the study area were also taken into account. The temperature field is then used as input for the rheological model in order to derive the best fit for the CEBS.

Numerical modelling

Many studies in the past have related large-scale deformations to geodynamical causes. Failing to reproduce local features has led to a large number of studies on modes of lithospheric deformation as a function of its rheological structure. We performed several numerical “tectonic deformation experiments” in order to explore the consequences of compositional and thermal parameters. Our goal is the quantification of the impact of rheology on the tectonic deformation and stress setting. Here follows a brief description of the procedure followed and then the main results are discussed.

Case 1: Impact of the sedimentary fill

Model assumptions

To consider the impact of the thermal blanketing of the sedimentary fill, the sediments were modelled as a single vertical layer with a rheology very close to salt. Table 1 illustrates the model creep parameters, while Fig. 6 shows the sediment thickness map used in all calculations. It was adapted to our study area from the depth-maps published by Scheck-Wenderoth and Lamarche (2005). Its main features can be summarized as follows: there are two directions of depocentre axes, (1) NW-SE-trending with maxima under the Permian Basins and (2) N-S-trending just above the Mesozoic grabens. It images a complex pattern of lows and highs. The basin is framed by the Tornquist Zone in the north and the EFS in the south. The presence of the Ringkøbing-Fyn-High is also represented in the map. In this case study, the other structures comprise a single layered crust overlying a mantle of constant depth of 100 km. The Moho boundary is shown in Fig. 4b. Different models have been performed with creep parameters representing granite, granodiorite, felsic-granulite, diabase and quartzite crustal rocks, while the mantle was imagined with an olivine or a dunite dominated rheology (see Table 1 for the reference parameters).

Table 1 Creep parameters of the rocks used in the modelling study (Ranalli 1995; Chopra and Peterson 1981)

Type of rocks	$\dot{\epsilon}_0$ (Mpa ⁻ⁿ s ⁻¹)	E (kJ mol ⁻¹)	n
Salt	6.3	102	5.3
Quartzite (dry)	6.7×10^{-6}	156	2.4
Diabase (dry)	2.0×10^{-4}	260	3.4
Felsic granulite (dry)	8.0×10^{-3}	243	3.1
Mafic granulite (dry)	1.4×10^4	445	4.2
Olivine (dry)	2.4×10^4	532	3.5
Dunite (dry)*	6.3×10^{-2}	444	3.41
Granite (dry)	1.8×10^{-9}	123	3.2

Results

Despite the differences in rocks properties, the models showed the same general pattern, and therefore we illustrate and discuss only one example. In this case the crust has a quartzite dominated rheology, while the mantle is characterized by olivine creep behaviour (see Table 2 for the thermal parameters used). Figure 7 illustrates the results obtained in terms of strain rates and the deformation velocity field. The model resembles the reference deformation pattern shown in Fig. 2. An overall extensional setting oriented, mainly NW-SE characterizes the north-eastern part of the domain where almost no sediments are presented, while a compressional deformation style, NE-SW-oriented, becomes comparable to extension or even dominant in the south-west part of the study domain. The inclusion of the sedimentary fill proves to induce higher strain-rate eigenvalues without affecting the deformation style. As major effect the sediments weaken the lithosphere. This is due to their low value of thermal conductivity causing high temperatures in the upper part of the

Table 2 Values of the parameters used in the thermal modelling (see text for discussion)

Layer	Density (kg m ⁻³)	Heat production (W m ⁻³)	Thermal conductivity (W m ⁻¹ K ⁻¹)
Sediments	2,200	9.7×10^{-7}	2.2
Crust	2,850	1.5×10^{-7}	2.5
Mantle	3,300	0.0	3.4

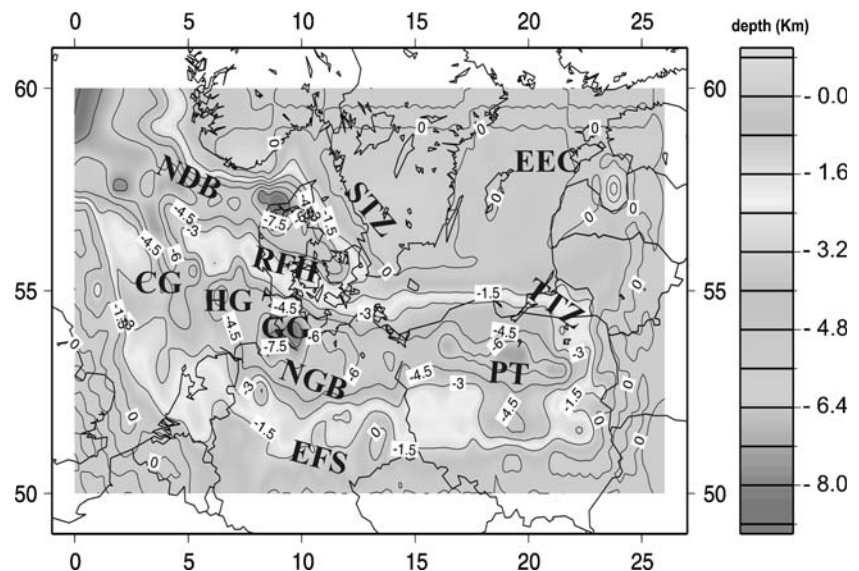
plate (Ziegler et al. 1998; Cloetingh and Van Wees 2005). This weakening effect leads to the formation of wide areas prone for strong deformation, (see Fig. 7) with increased strain rate values in the region covered by sediments.

Case 2: Shallow mantle thermal effects

Model assumptions

For reproducing the shallow mantle discontinuities, the lithosphere was no longer considered as a plate of constant thickness. For modelling the mantle we followed the general results derived from the TOR project (Gregersen and Voss 2002; Voss et al. 2006). This large-scale seismic experiment was mainly concentrated on the deep lithosphere and asthenosphere, confirming the presence of large lateral transitions in the lithosphere of the CEBS. From the TOR results, the transition is considered to be sharp and steep in two places: (1) at the northern rim of the Tornquist Zone near the border between Sweden and Denmark where the lithosphere reaches depths of 200–250 km, and (2) near the southern edge of the Ringkøbing-Fyn-High where the difference becomes smaller, from 90–100 km of depth to 120–150 km. Figure 8 illustrates the depth map which we generated for the asthenosphere boundary. The parameters

Fig. 6 Map showing the depth of the sedimentary layer used in the thermal and rheological models. It is adapted to the study area from the base-map of the Zechstein published by Scheck-Wenderoth and Lamarche (2005). The main elements presented are: (1) East European Craton (EEC). (2) Sorgenfrey-Tornquist-Zone (STZ). (3) Teysserie-Tornquist-Zone (TTZ). (4) Polish Trough (PT). (5) Ringkøbing-Fyn-High (RFH). (6) Norwegian-Danish Basin (NDB). (7) Central Graben (CG). (8) Horn Graben (HG). (9) Glückstadt Graben (GG). (10) North German Basin (NGB). (11) Elbe Fault System (EFS)



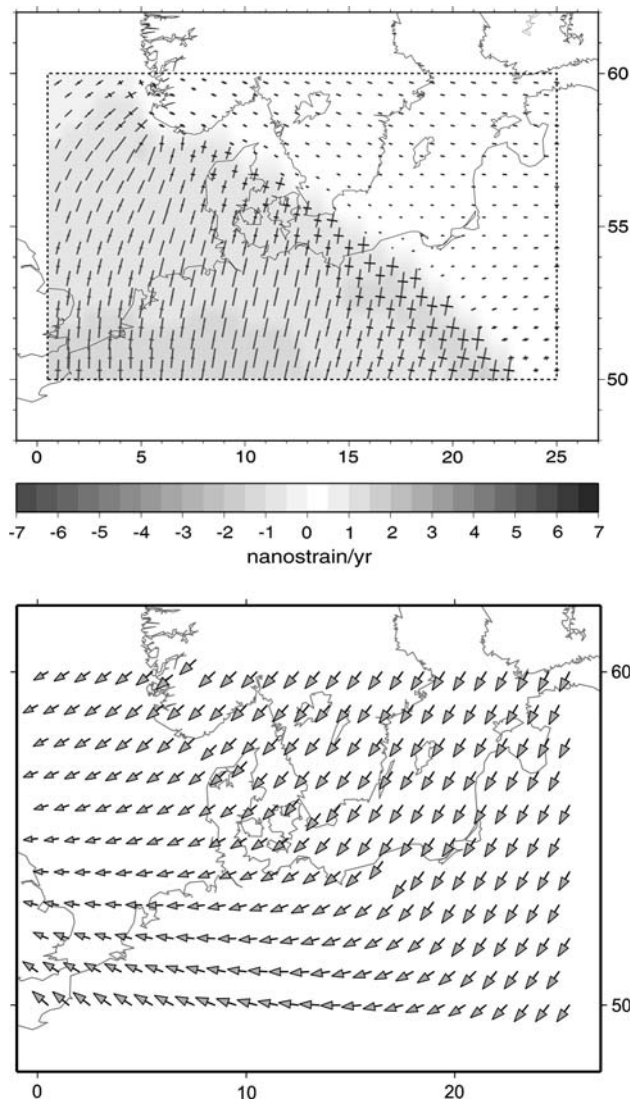


Fig. 7 Strain rates (*upper figure*) and horizontal velocity field (*lower figure*) obtained only considering the sedimentary thermal blanketing (*light background indicates extension, and dark background compression*). There is a general agreement with the reference model depicted in Fig. 2

used for reproducing the rheology of the sedimentary layer, the crust and the mantle were the same as in Case 1: salt, quartzite and olivine, in order to isolate and quantify shallow mantle thermal effects. The depth map of the asthenosphere (Fig. 8), illustrates three domains within the study area: (1) a relative weak Variscan domain in the south and south-west; (2) a stiff and strong lithosphere beneath the EEC in the east and north-east, and (3) a transition zone extending between these two areas.

Results

The obtained results reproduce the overall scenario observed after the Late Cretaceous–Early Tertiary Alpine

orogeny, when the region between the Sorgenfrey-Tornquist-Zone and the Elbe Line accommodated the main inversion structures, with normal faults being reactivated as reverse faults. The model now generates strong strain localization concentrated along the transition domain (see Fig. 9). The reproduced rheological heterogeneities affect the direction of the strain-rate eigenvectors leading to changes in the azimuth of the eigenvectors. The presence of a stiffer lithosphere below the transitional domain along the asthenosphere boundary acts as a barrier preventing a release of deformation for the area south of it. Coherent with the boundary conditions imposed along the southern border of the domain, compression is mainly NW-SE-directed providing better agreement with geodetic observations (Fig. 2). Moreover, the results demonstrate that rheological heterogeneities are able to induce changes in the eigenvalues of the strain-rate tensor. As a consequence, the domain between the Elbe Line and the Tornquist Zone is now characterized by higher strain rate eigenvalues. Furthermore, the region of the Polish Trough shows a change in deformation style with a transition from a compressive dominated regime to an extensional one. In order to better constrain the results, the predicted direction of the maximum horizontal stress component, S_{Hmax} , (Fig. 10) was compared with the observed data (Fig. 3). The actual World Stress Map (Reinecker et al. 2005) shows a uniform pattern of WNW-ESE-directed maximum horizontal compressive stress in North Europe with a clockwise rotation toward ENE-WSW in the north-eastern part of Germany and Poland. The calculated largest horizontal stress field reproduces the fan-like structure only within a limited area. The predicted change in the direction of the largest horizontal stress is localized only in the northeast part of the North German Basin and in the southernmost part of the Polish Trough. The results of Fig. 10 show a mismatch between the predicted and the observed S_{Hmax} in the westernmost onshore part of Denmark and below the Danish sector of the Central North Sea Graben, dashed framed region of Fig. 10. Within these areas our results image a NE-SW-oriented maximum horizontal stress component which is almost perpendicular to the observed WNW-ESE-oriented S_{Hmax} . The local mismatch found between the model predictions and the observations may be directly related to the particular composition of the lithosphere in those areas.

Case 3: Lateral rheological heterogeneities in the crust

Model assumptions

In order to reproduce lateral changes in geophysical properties, the crust was split into two layers. At this point the vertical structures comprise: (1) the sediments with a

Fig. 8 Map showing the lithosphere–asthenosphere isothermal boundary as derived from the TOR experiments results (Gregersen and Voss 2002)

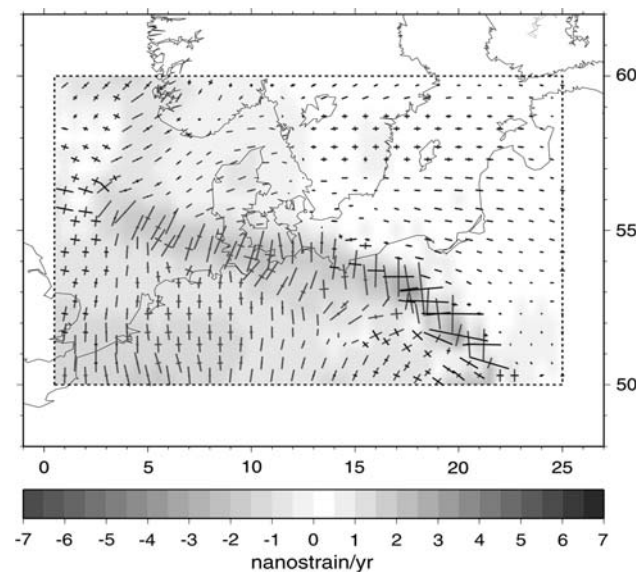
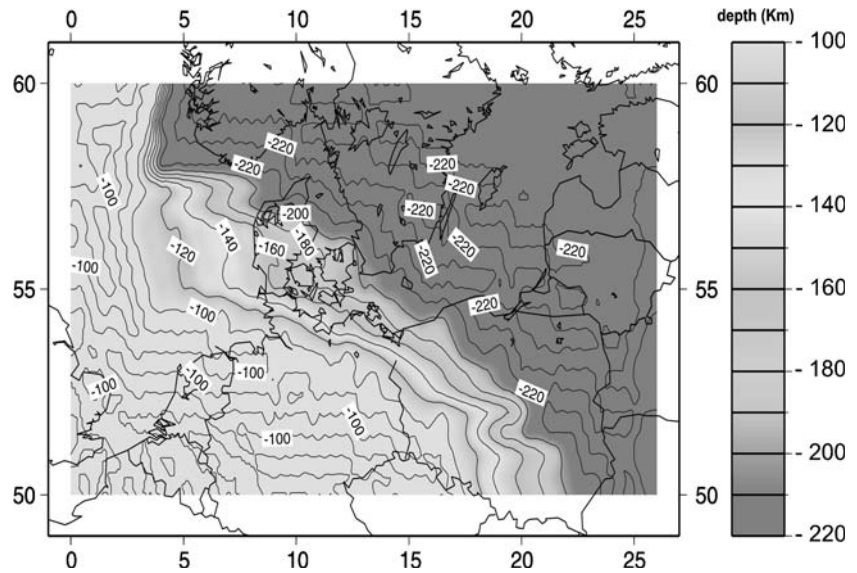


Fig. 9 Maximum horizontal strain rate as predicted by the model discussed in Case 2. As a consequence of having considered a transition domain in the lithospheric mantle, the deformation, mainly compression, is now focused along this area

salt-driven rheology, see Fig. 7 for the depth map; (2) the upper crust with a quartzite or granite rheology and a lower boundary at oscillating depth between 20 and 30 km according to seismic results; (3) a lower crust down to the Moho (Fig. 4b), for which several rheological analogues were implemented; and (4) a mantle of variable thickness (Fig. 8) with an olivine dominated behaviour. As second step, for modelling lateral structural contrasts, we subdivided the whole area into four domains (Fig. 11) with different rheologies in the lower crust. Our choices for the rheological analogues were based on results derived from

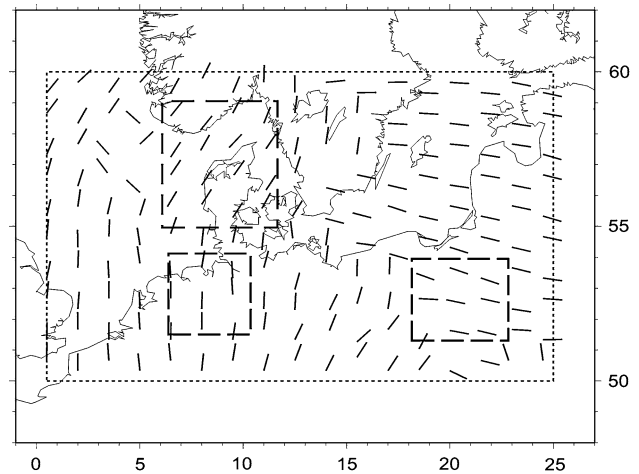


Fig. 10 Map showing the direction of the maximum horizontal stress component, S_{Hmax} , as predicted by the model discussed in Case 2. The areas framed by dashed quadrates are those where the strongest disagreement was found

local studies. The range of P-wave lower crustal velocities ($6.2\text{--}6.5\text{ km s}^{-1}$) and densities ($2,700\text{--}2,800\text{ kg m}^{-3}$) observed in the area along the Elbe Fault System motivated a granitic to a granodioritic dominant composition. The high values for P-wave velocities reaching $6.9\text{--}7.0\text{ km s}^{-1}$ and the range of densities ($2,900\text{--}3,100\text{ kg m}^{-3}$) in the lower crust north of the Elbe River and below the Sudetes in Poland suggest a lithology typical for gabbros. Finally, we modelled this area with a felsic-granulite composition. To the north this felsic-granulite composed lower crust is bounded by the Tornquist Zone. For the Baltic region we used a slightly stronger mafic-granulite rheology. For the area south of the Elbe Fault system we considered three cases. First the lower crust was modelled with a granodi-

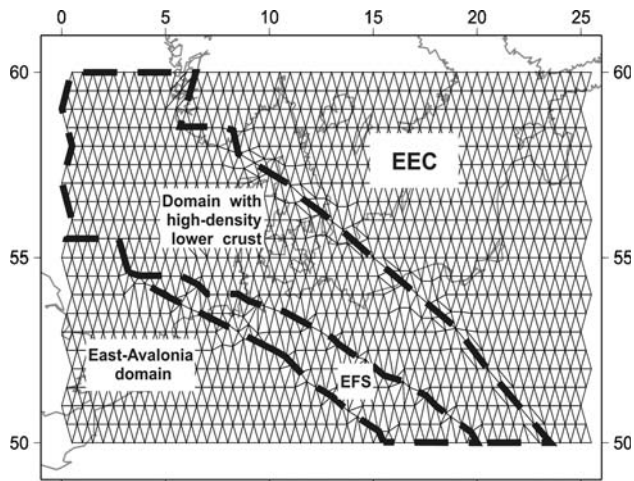


Fig. 11 2-D grid used for the integral model as discussed in Case 3. The lateral domains with different rheological properties in the lower crust are shown

orite dominant lithology, resembling a weak crustal body. A quartzite composition and a diabase dominated composition were chosen respectively for the second and the third experiments, reproducing a stronger crust. Table 3 summarizes the different data used for the simulations.

Results

We limit the discussion to three examples (Model 2, Model 4 and Model 6 of Table 3) because the best results were obtained by modelling the upper crustal layer with a dominant quartzite rheology. Figures 12, 13 and 14 illustrate the resulting strain rates. Despite different rheologies used for modelling the Variscan domain, the models generated the same trend, therefore we discuss them together. The main feature shown in the figures is a southward shift of the zone of strain localization. Now, the area with highest deformations is found below the EFS, while a minor compression is still visible along the Tornquist Zone. The lithosphere is weaker beneath the EFS than below the surrounding areas due to the granitic composition in the lower crust which provides increased temperatures. This weakness explains the observed strain localization under this region. The introduction of lateral contrasts improves the results in those locations where the strongest mismatch was found before, maintaining at the same time the overall consistency between the model and observations. The kinematical scenario for the North German Basin is now in agreement with its recent compressional phase and the present-day setting. N-S to NNE-SSW-oriented compression is stronger in the weaker crust below the EFS rather than in the northern part where the predicted strain rate pattern indicates low deformation rates. This aspect is in agreement with the observed local aseismicity of the

Table 3 List of models considered in the analysis

Layer	Horizontal subdivision	Rheology	Model number
Sediments	None	Salt	1
Upper crust	None	Granite	
Lower crust	East-Avalonia High density body Baltic Shield EFS	Quartzite Felsic-Granulite Mafic-Granulite Granite	
Mantle	None	Olivine	2
<i>Sediments</i>	<i>None</i>	<i>Salt</i>	
<i>Upper crust</i>	<i>None</i>	<i>Quartzite</i>	
<i>Lower crust</i>	<i>East-Avalonia High density body Baltic Shield EFS</i>	<i>Quartzite Felsic-Granulite Mafic-Granulite Granite</i>	3
<i>Mantle</i>	<i>none</i>	<i>Olivine</i>	
<i>Sediments</i>	<i>None</i>	<i>Salt</i>	
<i>Upper crust</i>	<i>None</i>	<i>Granite</i>	4
<i>Lower crust</i>	<i>East-Avalonia High density body Baltic Shield EFS</i>	<i>Felsic-Granulite Felsic-Granulite Mafic-Granulite Granite</i>	
<i>Mantle</i>	<i>None</i>	<i>Olivine</i>	
<i>Sediments</i>	<i>None</i>	<i>Salt</i>	5
<i>Upper crust</i>	<i>None</i>	<i>Granite</i>	
<i>Lower crust</i>	<i>East-Avalonia High density body Baltic Shield EFS</i>	<i>Granite Felsic-Granulite Mafic-Granulite Granite</i>	
<i>Mantle</i>	<i>None</i>	<i>Olivine</i>	6
<i>Sediments</i>	<i>None</i>	<i>Salt</i>	
<i>Upper crust</i>	<i>None</i>	<i>Quartzite</i>	
<i>Lower crust</i>	<i>East-Avalonia High density body Baltic Shield EFS</i>	<i>Granite Felsic-Granulite Mafic-Granulite Granite</i>	
<i>Mantle</i>	<i>None</i>	<i>Olivine</i>	

The text in italics enlighten the models will be discussed in details

region, suggesting a rather undeformable area in the northern part of the basin. The results of Figs. 12, 13 and 14 show a change in deformation patterns within the area of the Polish Basin which is now characterized by a N-

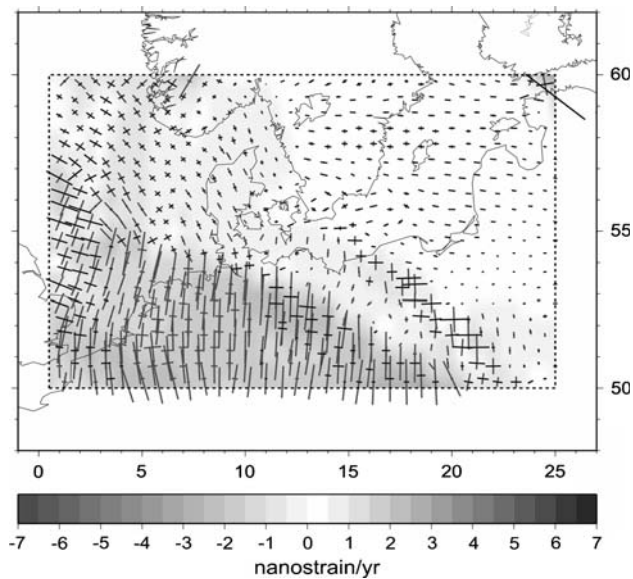


Fig. 12 Predicted strain-rate eigenvectors for Model 2 of Table 3 (light background indicates extension and dark background compression)

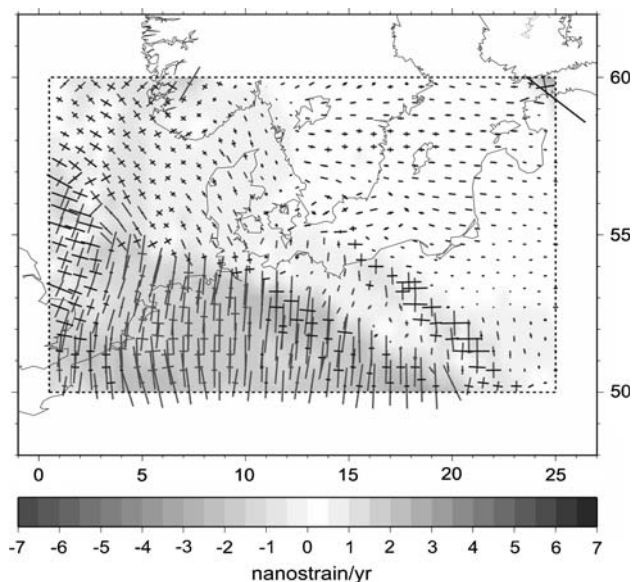


Fig. 13 Strain-rate eigenvectors predicted by Model 4 of Table 3

S-oriented to a NWN-SES-oriented compression. This variation in the deformation patterns indicates that lateral rheological heterogeneities can affect the azimuth of the strain-rate eigenvectors as well as the related eigenvalues. Moreover, the presence of the high-density lower crust below the Polish Trough has moved the centre of maximum strain localization from the TTZ southward. This scenario is in agreement with the present-day tectonic setting of this region which is dominated by a collision-induced compressive intra-continental stress pattern with

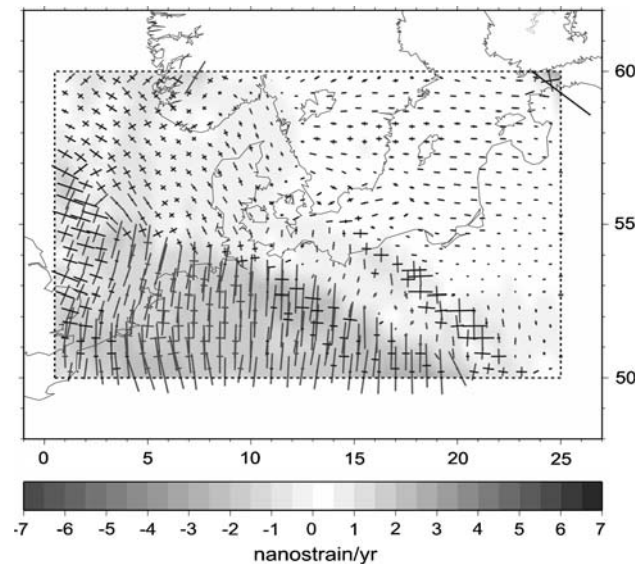


Fig. 14 Strain-rate eigenvectors obtained from Model 6 of Table 3

the main depocentres located in its southernmost part. The predicted orientation of the principal horizontal compressive stress (Figs. 15, 16 and 17) shows a general agreement with the present-day stress pattern observed over North Central Europe (Zoback 1992; Reinecker et al. 2005). The modelled stress field images the overall NW-SE-oriented principal axes and also the progressive rotation to S-N/NE in the eastern part of the study region. Focusing on the NGB where many previous studies have failed in predicting the stress field orientation, our results are consistent with the observation showing the fan-like pattern in the direction of S_{Hmax} . Lateral heterogeneities induce changes in the magnitude of the stress tensor as well as in its orientation being able to resemble more local features. Furthermore, the predicted stress regime suggests that the north-easternmost area of the North German Basin is still in a state of horizontal compression, having not yet reached isostatic equilibrium as derived by Marotta et al. (2002). In a regional contest, an overall agreement between the predicted and the observed regional stress field is evident, although there is still a region of mismatch. In fact, the model fails in reproducing the orientation of the S_{Hmax} at its western boundary where it images a NE-SW-oriented maximum stress instead of a NW-SE-oriented one. This can be related to the particular boundary conditions applied along that border, i.e. a pure boundary effect.

Final remarks

A number of models have been presented to test the relative contribution of variations of compositional and thermal parameters to the setting of the regional stress field and

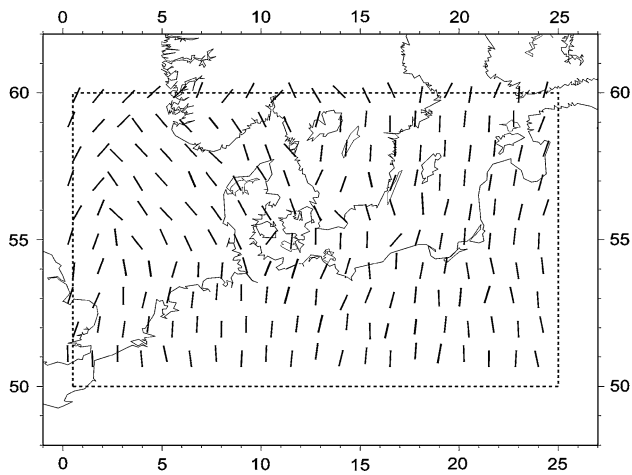


Fig. 15 Predicted direction of the maximum horizontal compressive stress, S_{Hmax} . The illustration refers to the case in which a quartzite-type lower crust was chosen for modelling the domain extending eastward the EFS (Model 2 of Table 3)

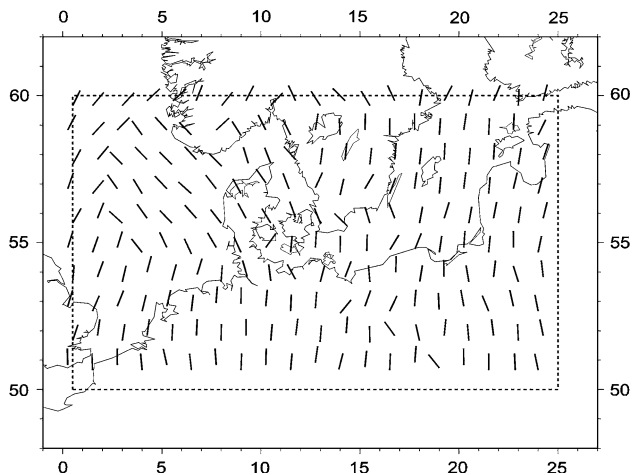


Fig. 16 Direction of S_{Hmax} with a felsic-granulite dominated rheology in the lower crust below the eastern part of the study domain (Model 4 of Table 3)

deformation pattern in the CEBS. The first sets of models (Case 1 and Case 2) were mainly focused on the evaluation of the effects induced by thermal fluctuations on the predicted stress field and strain pattern. These models resembled the overall features. On the other hand, the introduction of lateral crustal structural heterogeneities is necessary to explain more local features, as shown in Case 3. The presence of lateral contrasts induces changes in the direction of the strain-rate eigenvectors as well as in their related magnitudes. Moreover, lateral rheological heterogeneities affect the direction of the maximum component of the stress tensor. Our results suggest that rheology is a first order driving element for deformations and stresses even in tectonic scenario like the CEBS which are almost dominated by boundary forces.

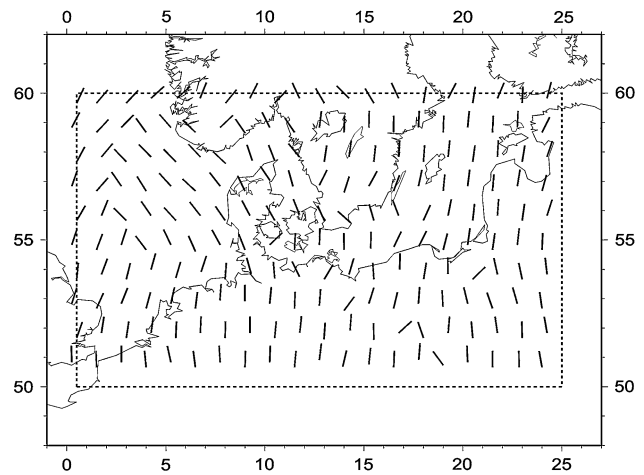


Fig. 17 Predicted S_{Hmax} direction for a granite dominated rheology along the eastern part of the study region (Model 6 of Table 3)

Conclusions

A viscous thin sheet model has been used to investigate the role of rheological contrasting structures on deformation and stresses focusing on the area of the CEBS. Unlike many previous integral studies, the effects of variations in the thermal regime have been considered in order to determine the best fitting rheologies for different sub-domains. The consistency of the results has been constrained by direct comparisons of the model outcomes and two independent sets of data. For this purpose, the reference parameters are the present-day regional stress field obtained from the “World stress Map Project” (Reinecker et al. 2005) and the strain rate eigenvectors derived by the last ten year GPS observations of the ITRF2000 database (Altamini et al. 2002). The results demonstrate that the observed deformation and stress pattern in the CEBS can be reproduced with reasonable agreement by the model, concerning the overall trend as well as more local features.

Concerning the deformation style, lateral rheological heterogeneities have been proved to induce variations in the azimuth of the strain-rate eigenvectors as already suggested by previous studies (e.g. Marotta 2005). On the other hand, lateral contrasts turn out to affect the strain-rate eigenvalues revealing their key role in stiffening the propagation of tectonic deformation in the CEBS. In a local contest, the obtained results reproduce a weak lower crust below the EFS and suggest a rather undeformable area in the northern part of the NGB, in agreement with previous results (e.g. Marotta et al. 2000).

In contrast to Golke and Coblenz (1996), we have demonstrated that the direction of the principal stress axes is not totally independent of the rheology of the lithosphere. The presence of different structural domains at crustal and shallow mantle level is responsible for the

present-day local variations observed in the direction of the regional stress field. Moreover, our results suggest a present-day state of horizontal compression in the easternmost part of the NGB. This feature is in agreement with previous models (Marotta et al. 2000; Marotta et al. 2002), with results from gravity studies (Scheck-Wenderoth et al. 1999), and with observations from deep seismic experiments (MONA-LISA Group 1997; DEKORP-BASIN Group 1999). The results have shown that strong strain localization and major deviation in the stress directions occur without considering pre-defined ‘a-doc’ faults as has been often used in this context (e.g. Kaiser et al., 2005). In contrast, the same results indicate that large inherited structures may play an important role in the evolution of complex basins controlling processes including strain localization which finally leads to failure and to faults formations. The best agreement between the results and the observations has been found when:

- The sedimentary layer is represented by a salt dominated rheology.
- Variations in the thickness of the lithosphere are modelled, considering a step-wise transition between the Elbe Line in the south and the Tornquist Zone in the north.
- The upper crustal layer is modelled with a stronger quartzite-like rheology rather than with a weaker granite dominated one.
- Lateral structural contrasts at lower crustal depth are considered. These discontinuities comprise the presence of (1) the high density body in the lower crust below north Germany, and (2) a relatively zone of weakness along the EFS.

Our analysis was focused on the influence of large-scale structures on stresses and deformation patterns. It demonstrated that a key factor for the distribution of the compressive stress and strain localization in the CEBS area is the presence of lateral rheological heterogeneities. Strong lateral contrasts are driving the propagation of tectonic deformation and affect the regional tectonic setting.

Acknowledgments The authors would like to acknowledge the German Research Council for its financial help, provided within the DFG-SPP 1135 ‘‘Dynamics of sedimentary systems under varying stress conditions by example of the Central European Basin System’’. We would like to thank Magdalena Scheck-Wenderoth for providing data concerning the sedimentary thicknesses and for her valuable comments. Special thank goes to Yuriy Maystrenko for all his help during the first draft of this paper, for providing us with other data set for the calculations and for his constructive review. We are grateful to the Geophysical Institute of Karlsruhe University, especially J. Reinecker, O. Heidbach, M. Tingay, B. Sperner, B. Müller, for providing the WorldStressMap-plots and to Ziegler P.A. and Dèzes P. for their European Moho depth map. All illustrations were made using GMT of Wessel and Smith (1998). Finally, the authors are thankful for the

helpful comments and suggestions of Professor Sierd Cloetingh and two others anonymous reviewers.

References

- Altamini Z, Silard P et al (2002) ITRF2000: a new release of the International Terrestrial Reference Frame for Earth Science applications. *J Geophys Res* 107:20001JB000561
- Bayer U, Scheck-Wenderoth M et al (1997) Modelling of the 3D thermal field in the northeast German basin. *Geol Rundsch* 86:241–251
- Bayer U, Scheck-Wenderoth M et al (1999) An integrated study of the NE German Basin. *Tectonophysics* 314:285–307
- Berthelsen A (1998) The Tornquist Zone northwest of the Carpathians: an intraplate pseudosuture. *Geol Stockh Förh* 120:223–230
- Bijwaard H, Spakman W et al (1998) Closing gap between regional and global travel time tomography. *J Geophys Res* 103:30055–30078
- Byerlee JD (1978) Friction of rocks. *Pure Appl Geophys* 116:615–626
- Chopra PN, Peterson MS (1981) The experimental deformation of Dunite. *Tectonophysics* 78:453–473
- Cloetingh S, Burov EB (1996) Thermomechanical structure of European continental lithosphere: constraints from rheological profiles and EET estimates. *Geophys J Int* 124:695–723
- Cloetingh S, Van Wees JD (2005) Strength reversal in Europe’s intraplate lithosphere: transition from basin inversion to lithospheric folding. *Geology* 33:285–288
- DEKORP-BASIN Group (1999) Deep crustal structure of the Northeast German Basin: new DEKORP-BASIN’96 deep profiling results. *Geology* 27:55–58
- Devoti R, Ferraro C et al (2002) Geophysical interpretation of geotectonic deformations in the Central Mediterranean area. *Tectonophysics* 346:151–167
- England P, Houseman G (1985) Role of lithospheric strength heterogeneities in the tectonic of Tibet and neighbouring regions. *Nature* 315:297–301
- England P, Houseman G (1989) Extension during continental convergence, with application to the Tibetan Plateau. *J Geophys Res* 94:17561–17579
- Gemmer L, Nielsen SB (2001) Three-dimensional inverse modelling of the thermal structure and implications for lithospheric strength in Denmark and adjacent areas of Northwest Europe. *Geophys J Int* 147:141–154
- Gregersen S, Voss P (2002) Summary of project TOR: delineation of a stepwise, sharp, deep lithosphere transition across Germany-Denmark-Sweden. *Tectonophysics* 360:61–73
- Golke M, Coblenz D (1996) Origins of the European regional stress field. *Tectonophysics* 266:11–24
- Goes S, Loohuis JJP et al (2000) The effect of plate stresses and shallow mantle temperatures on tectonics of northwestern Europe. *Glob Planet Change* 27:23–38
- Goetze C, Evans B (1979) Stress and temperature in the bending lithosphere as constrained by experimental rock mechanics. *Geophys J R Astron Soc London* 135:463–478
- Guterch A, Grad M et al (1999) POLONAISE’97—an international seismic experiment between Precambrian and Variscan Europe in Poland. *Tectonophysics* 314:101–121
- Jiménez-Munt I, Garcia-Castellanos D et al (2005) Thin-sheet modelling of lithospheric deformation and surface mass transport. *Tectonophysics* 407:239–255
- Kaiser A, Reicherter et al (2005) Variation of the present-day stress field within the North German Basin—insights from thin shell FE modelling based on residual GPS velocities. *Tectonophysics* 397:55–72

- Krawczyk C, Eilts F et al (2002) Seismic evidence of Caledonian deformed crust and uppermost mantle structures in the northern part of the Trans-European Suture Zone, SW Baltic Sea. *Tectonophysics* 360:215–244
- Lankreijer A, Mocanu V et al (1997) Lateral variations in lithosphere strength in the Romanian Carpathians: constraints on basin evolution. *Tectonophysics* 272:269–290
- Lockhorst A (1998) NW European Gas Atlas-Composition and Isotope ratios of Natural Gases. Gis application on CD by the British Geological Survey, Bundesanstalts für Geowissenschaften und Rohstoffe, Danmarks og Grolnlands Geologiske Undersogelse, Nederlands Instituut voor Toegepaste Geowetenschappen, Panstwowy Instytut Geologiczny, European Union
- Lynch HD, Morgan P (1987) The tensile strength of the lithosphere and the localization of extension. *Geol Soc Spec Publ* 28:53–65
- Majdanski M, Grad M et al (2006) 2-D seismic tomographic and ray tracing modelling of the crustal structure across the Sudetes Mountains basing on SUDETES 2003 experiment data. *Tectonophysics* 413:249–269
- Marotta AM, Bayer U et al (2000) The Legacy of the NE German Basin-reactivation by compressional buckling. *Terra Nova* 12:132–140
- Marotta AM, Bayer U et al (2002) Origin of the regional stress in the North German basin: results from numerical modelling. *Tectonophysics* 360:245–264
- Marotta AM, Sabadini R (2003) Numerical models of tectonic deformation at the Baltica-Avalonia transition zone during the Paleocene phase of inversion. *Tectonophysics* 373:25–37
- Marotta AM, Mitrovica JX et al (2004) Combined effects of tectonics and glacial isostatic adjustment on intraplate deformation in central and northern Europe: applications to geodetic baseline analyses. *J Geophys Res* 109:B01413
- Marotta AM (2005) The fingerprints of intra-continental deformation in Central Europe as envisage by the synergic use of predicting modelling and geodetic data. *Bollettino Geofisica Teorica Applicata* 46:181–199
- Mattern F (1996) the Elbe Zone at Dresden—a late paleozoic pull-apart intruded shear zone. *Z Dtsch Geol Ges* 147:57–80
- Maystrenko Y, Bayer U et al (2005) The Glückstadt Graben, a sedimentary record between the North and Baltic Sea in north and central Europe. *Tectonophysics, Special Issue* 397:113–126
- McClusky S et al (2000) Global positioning system constraints on plate kinematics and dynamics in the eastern Mediterranean and Caucasus. *J Geophys Res* 105:5695–5719
- Molnar P, Tapponier P (1981) A possible dependence of the tectonic strength on the age of the crust in Asia. *Earth Planet Sci Lett* 52:107–114
- MONA-LISA Group (1997) the closure of the Tornquist Sea: constraints from MONA LISA deep seismic reflection data. *Geology* 25:1071–1074
- Ranalli G (1995) *Rheology of the Earth* 2nd ed. Chapman and Hall
- Reinecker J, Heidbach O, Tingay M, Sperner B, Müller B (2005) The release 2005 of the World Stress Map. Available online at: <http://www.world-stress-map.org>
- Richardson RM, Solomon SC, Sleep NH (1979) Tectonic stress in the plates. *Rev Geophys* 17:981–1019
- Scheck-Wenderoth M, Bayer U (1999) Evolution of the Northeast German Basin-inferences from a 3D structural model and subsidence analysis. *Tectonophysics* 313:145–169
- Scheck-Wenderoth M, Bayer U et al (2002) The Elbe Fault system in North Central Europe—a basement controlled zone of crustal weakness. *Tectonophysics* 360:281–299
- Scheck-Wenderoth M, Lamarche J (2005) Crustal memory and basin evolution in the Central European Basin System-new insights from a 3D structural model. *Tectonophysics* 297:281–299
- Tomasi A, Vauchez A et al (1995) Initiation and propagation of shear zones in a heterogeneous continental lithosphere. *J Geophys Res* 100:22083–22101
- Turcotte D, Schubert G (2002) *Geodynamics*, 2nd edn. Cambridge University Press
- Yegorowa T, Bayer U et al (2007) Gravity signals from the lithosphere in the Central European Basin System (in press)
- Vejbaek O (1997) Dybe strukturer i danske sedimentære bassiner. *Geol Tidsskr* 4:1–31
- Voss P, Mosegaard K et al (2006) The Tornquist Zone, a north east inclining lithospheric transition at the south western margin of the Baltic Shield: revealed through a nonlinear teleseismic tomographic inversion. *Tectonophysics* 416:151–166
- Weertman J, Weertman JR (1975) High temperature creep of rock, and mantle viscosity. *Ann Rev Earth Planet Sci* 3:292–315
- Wessel P, Smith WHF (1998) New improved version of the generic mapping tools released. *EOS Trans. AUG* 79:579
- Ziegler PA (1990) *Geological Atlas of Western and Central Europe*, 2nd edn. Shell International/Geol Soc Publ House, London, p 239
- Ziegler PA, Van Wees JD et al (1998) Mechanical controls on collision-related compressional intraplate deformation. *Tectonophysics* 300:103–129
- Ziegler PA, Dézes P (2005) *Crustal evolution of Western and Central Europe*. Memoir of the Geological Society, London
- Zoback ML (1992) First-and-second-order patterns of stress in the lithosphere. The World Stress Map Project. *J Geophys Res* 97:11703–11728